EMI Diagnostics of Three Phase Inverters Using Machine Learning Algorithms

Matthew Boubin[+], John Patrick Doran, Wilson Guo, Yamuna Rajasekhar, Mark Scott[*]
Department of Electrical and Computer Engineering
Miami University
Oxford, Ohio U.S.A.
[+]: boubinmj@miamioh.edu
[*]: scottmj3@miamioh.edu

***Abstract*—Electromagnetic interference (EMI) is often regarded as a disturbance in electrical systems, and most research focuses on developing techniques to mitigate its impact. EMI is particularly problematic in many sensing applications, but there are circumstances when EMI can be used as the sensing tool. This paper describes a method to determine the health of the DC link capacitance in a three-phase inverter using EMI diagnostics. The proposed approach relies on changes in a capacitor's resonant frequency and impedance, which occur naturally as it ages, to predict its health. These parameters influence the conducted EMI measurements in a manner that is detectable. Through simulation and experimentation, it is demonstrated that this approach can detect changes in a capacitor's health via a machine learning algorithm that is trained to inverters EMI spectrum.**

***Index Terms*—electromagnetic interference, machine learning, diagnostics, DC link capacitor, support vector machine, common mode noise, differential mode noise**

I. Introduction

In the commercial airline industry, maintenance accounts for 10% to 20% of the total operating costs for an aircraft and this equals, on average, $3.6 M per aircraft per year [1]. Additionally, as much as 40% of equipment is falsely diagnosed and removed as the result of ambiguous and labor intensive test procedures [1], [2]. More precise and effective methods of diagnosing problems are needed to reduce these costs.

Because existing diagnostics procedures are expensive, there is a growing interest in non-invasive diagnostic methods that provide users with real-time information about the status of electrical systems [3]–[5]. Several methods have been proposed for electric machines [3]–[8]. Casadei et al. [7] propose a field oriented control method that enables them to identify demagnetization of the rotor magnets. Their procedure monitors the emfs harmonic content looking for variations in the seventh and ninth harmonics. Wolbank et al. [8] created a non-invasive test procedure to detect rotor winding damage in a squirrel cage induction machine. Prior to operation, the inverter applies voltage steps to the stator and uses the control loop current sensors to identify asymmetries in the transient flux.

Another method is to utilize the spectrum of the electromagnetic interference (EMI) to analyze the systems health. EMI is very sensitive to changes in device parameters. As failure mechanisms emerge, changes manifest themselves in the spectrum. By properly cataloging this phenomenon, measurement techniques can detect hardware issues in their early stages of development prior to actual component failure [3]. Since the 1980s, this method has been utilized to evaluate the health of electrical systems [3]–[5]. Numerous conditions can be identified using a radio frequency current transformer on the neutral wires of electrical devices. Previous authors have been able to detect improper grounding, broken rotor bars, and loose connections in a transformer as well as conductor related defects [3], [5]. The sensitivity of EMI and its non-invasive measurement method make it a strong candidate for performing in situ diagnostics of power electronics.

In this hardware, semiconductor switching devices and DC link capacitors, especially aluminum electrolytic capacitors, are some of the least reliable elements [9]. The conditions in an electric vehicle (EV) are quite extreme, and the change in the DC link capacitors behavior as it ages is significant enough to affect the performance of the vehicle [10]. One method that has not received a lot of attention is the use of an EMI spectrum to characterize the health of power electronics. This paper applies this technique to monitor the health of the DC link capacitor in a three phase inverter. However, circuit analysis confirms that this method diagnoses the health of other elements in the system like the semiconductor devices.

The following paper describes a method to use EMI diagnostics to assess the health of the DC link capacitance in a three phase inverter. The inverter was selected for this research because it is broadly applied in aviation, automotive applications, renewable energy, and telecommunication power systems. Section II provides the background information relevant to this research. This includes an equivalent circuit of a capacitor and the simplified EMI model of the inverter. In section III, a high level discussion on machine learning is provided. Section IV contains the description of the experimental procedures. In section V, the analysis of the results is presented. The final section of the paper concludes this research and presents future work.

978-1-4799-7312-5/18/$31.00 ©2018 IEEE

II. Background

This section begins with a review of the equivalent circuit of a capacitor to facilitate the discussion on EMI diagnostics. It uses this model to demonstrate how the impedance changes with age. Next, this model is inserted into a simplified inverter circuit to predict the EMI behavior of an inverter. The two are combined together to estimate how the EMI spectrum is effected by changes in the DC link's parameters.

A. DC Link Capacitor Model

DC link capacitors absorb semiconductor-switching noise, buffer the DC bus, and mitigate the ripple current seen by the DC source. Film capacitors are the most commonly used type of capacitors in EV inverters due to their ability to handle high RMS currents [11]. DC link capacitor failure in an EV inverter is a serious concern, and much research has gone into creating more resilient capacitors [12]. In EVs, DC link capacitors are at risk of being exposed to high temperatures, changes in humidity, and other external factors that could cause them to wear out or fail more easily than in other power electronics applications [13].

The model of a non-ideal capacitor is shown in Fig. 1. The capacitor (C_{DC}) is in series with two parasitic elements. The equivalent series resistance (R_{ESR}) models the resistance of the capacitor's electrodes, and the equivalent series inductance (L_{ESL}) represents their corresponding inductance. More complex models exist to emulate other non-ideal behaviors of the capacitor [13], but their impact on EMI is not treated in this paper.

The values of C_{DC} and R_{ESR} change as capacitors age [13]. Overvoltages cause localized breakdowns in the dielectric that result in momentary short circuits between the electrodes. The self-healing capability of a film capacitor eliminates this short circuit by vaporizing the conductive surfaces at the location of the short circuit and clearing the breakdown. A small loss of capacitance occurs because portions of the electrical layers and dielectric are destroyed. As these self-healing events accumulated over time, the DC link capacitance gradually degrades.

High currents in the capacitor lead to the demetallization of the electrodes and excess moisture inside the component corrodes the metalized layers of the capacitor [11]. The resulting loss of electrode material increases R_{ESR}, which increases loss inside of the capacitor. Both of these aging mechanisms reduce the effectiveness of the DC link capacitors and may move the associated power electronics out of compliance with relevant standards. Regarding L_{ESL} of the capacitor, it remains constant because the geometry of the capacitor does not change with capacitor age [14].

The complex impedance of the capacitor shown in Fig. 1 is:

$$Z = R_{ESR} + j\omega L_{ESL} + \frac{1}{j\omega C_{DC}} \tag{1}$$

where ω is the the angular frequency. The resonant frequency (f_r) of the capacitor occurs when the complex components cancel each other out. It is given as:

$$f_r = \frac{1}{2\pi\sqrt{L_{ESL}C_{DC}}}. \tag{2}$$

A plot of the impedance versus frequency for two classes of capacitors is shown in Fig. 2, and their corresponding values are given in Table I. The first class, *new capacitors*, has a higher capacitance and lower R_{ESR} than the *aged capacitors* set. From the plot, it is apparent that the impedance below the resonant frequency is higher for the aged capacitor. This is due to the higher R_{ESR} and lower C_{DC}. Above the resonant frequency, the impedance is roughly the same because L_{ESL} dominates. The resonant frequency of the aged capacitor is also higher than the new capacitor. Since the DC Link capacitance plays a critical role in filtering differential mode (DM) signals, it is expected that changes in the EMI spectrum will emerge for DM measurements.

B. EMI Model of a Three-Phase Inverter

A simplified schematic to model the EMI produced by a three-phase inverter is shown in Fig. 3 [15]. Two line impedance stabilization networks (LISN) are modeled using values for L_{LN}, C_{LN}, and R_{LN} that corresponds to those

Fig. 1. Equivalent circuit model of a DC link capacitor.

TABLE I
LCR values used for Fig. 2.

Class	*New Capacitors*	*Aged Capacitors*
C_{DC}	50 μF	40 μF
R_{ESR}	6 $m\Omega$	12 $m\Omega$
L_{ESR}	35 nH	35 nH

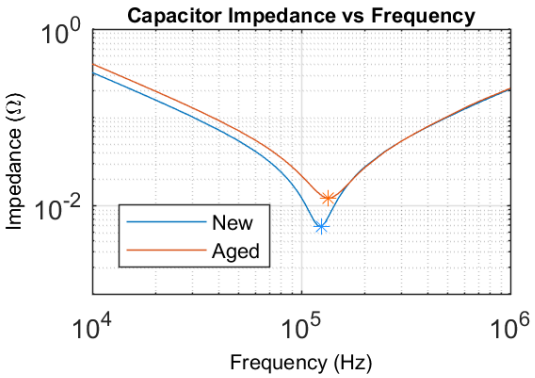

Fig. 2. Capacitor impedance vs. frequency for new and aged capacitors.

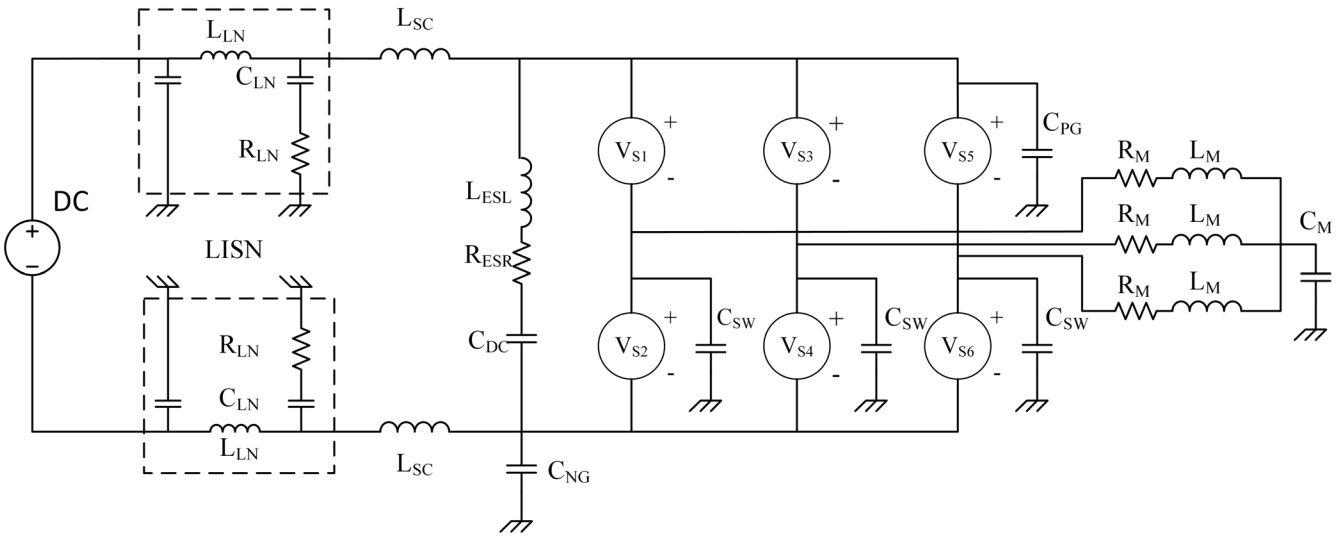

Fig. 3. Schematic of a three phase inverter used in simulation.

given in CISPR-25 [16]. The second order capacitor model in Fig. 1 is used for the DC link capacitors. The semiconductor devices are modeled as voltage sources ($V_{S,i}$). Parasitic capacitances couple the positive bus bar to the chassis (C_{PG}), the negative bus bar to chassis (C_{NG}), and each of the phases to the chassis ($C_{SW,i}$). A reactive load (R_M, L_M) is attached to the inverters output with a parasitic coupling capacitor (C_M) between the center point and ground.

Through manipulating the schematic in Fig. 3, the simplified circuit shown in Fig. 4 is created to model the DM noise [15]. The switches are modeled as pulsating current sources (I_{INV}) with specified rise and fall times that correspond with the physical semiconductor devices. The transfer function for the differential mode noise (V_{DM}) is derived using circuit analysis. The circuit is first simplified into three impedances, with $s = j\omega$:

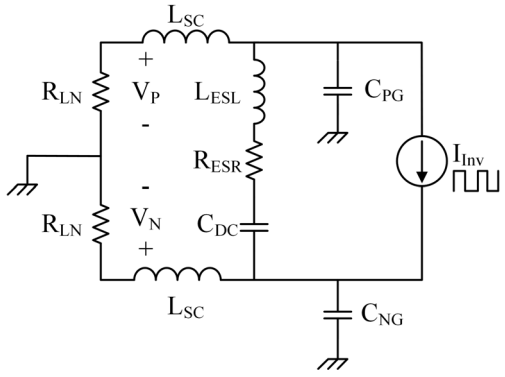

Fig. 4. Equivalent circuit of DM noise propagation paths in a three phase inverter.

$$Z_1 = \frac{(R_{LN} + sL_{SC})(\frac{1}{sC_{PG}})}{R_{LN} + sL_{SC} + \frac{1}{sC_{PG}}} \tag{3}$$

$$Z_2 = \frac{(R_{LN} + sL_{SC})(\frac{1}{sC_{NG}})}{R_{LN} + sL_{SC} + \frac{1}{sC_{NG}}} \tag{4}$$

$$Z_3 = R_{ESR} + sL_{ESL} + \frac{1}{sC_{DC}}. \tag{5}$$

Using (3), (4), and (5) the voltage drop across the LISNs' resistors are:

$$V_P = \frac{R_{LN}}{R_{LN} + sL_{SC}} \left(Z_1 \left(\frac{Z_3}{Z_1 + Z_2 + Z_3} \right) \right) I_{INV}(s) \tag{6}$$

$$V_N = \frac{R_{LN}}{R_{LN} + sL_{SC}} \left(-Z_2 \left(\frac{Z_3}{Z_1 + Z_2 + Z_3} \right) \right) I_{INV}(s). \tag{7}$$

From (6) and (7):

$$V_{DM} = \frac{V_P - V_N}{2}. \tag{8}$$

Changes in the DC link capacitor only effect the impedance of Z_3, which then impacts V_{DM}. The largest difference between the two capacitor cases is at the resonant frequency. At frequencies above the resonant frequency, the magnitude of the transfer function is very similar due to the inductive reactance overpowering the capacitance reactance (see Fig. 5). Below the resonant frequency, there is a slight offset with the aged capacitor having a higher impedance due to the R_{ESR}. As shown in Fig. 5, V_{DM} is sensitive to changes in the DC Link's parameters.

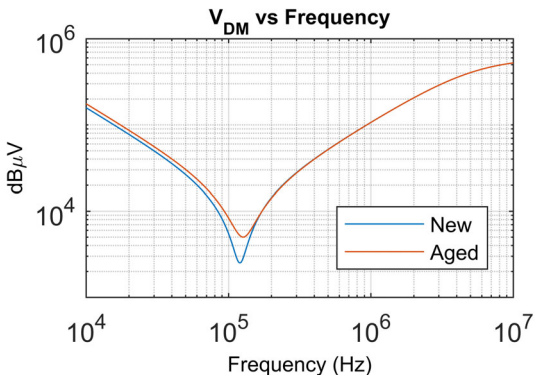

Fig. 5. DM voltage produce by inverter for two classes of capacitors.

C. Machine Learning

Support vector machine (SVM) learning is a regression based supervised learning model that is used to organize data sets into a finite number of classes [17]. A data set, or data vector, is an aggregation of a larger data space, and it contains values that are characteristic of a particular data space. It is used to dimensionally reduce the data space, so that it can be described with a smaller amount of data. Each member of a data set is called a feature. Before an SVM can classify data sets, a training model that describes data sets from each class must be developed. A training model is created by compiling data sets with known classes together to generate support vectors that support a given class. In training, the SVM maps data sets, x_i, to a higher order dimensional space by using a kernel function. Using a training model based on a kernel function, the SVM classifies unsupervised datasets submitted in the same format as the data sets used to train the SVM. In this experiment, a model with two possible classes was created, although many more can be used in future iterations. The training model used in this experiment was generated using a radial basis function (RBF) kernel [17]. The RBF kernel function is described by:

$$K(x, x_i) = exp(\frac{-\gamma||x - x_i||^2}{\sigma}) \tag{9}$$

where x is the value describing the class, x_i is a data set of length i, σ is the standard deviation of x_i, and γ is a scaling parameter, which was chosen to be 0.5.

Data sets that are used for testing are compared to the training model, and the SVM classifies data sets into one of the defined classes. Since the correct class of the test data sets are known in this experiment, the accuracy of the SVM classification function can be determined. The classification function used by the SVM is described by (10) where a_i is the data scaling factor, y_i is a data set of length i used for testing, and b is the error offset constant:

$$f(x) = \Sigma_{i=0}^{N} a_i y_i K(x, x_i) + b. \tag{10}$$

Equation 10 mathematically describes how a data set, y_i, is tested against an already existing model, $K(x, x_i)$. The output $f(x)$ will resemble one of the class identifiers associated with the data sets used to train the model in (9).

III. Experimental Results

The following tests were conducted on a EMI test bench setup to follow CISPR-25's guidelines. A three-phase inverter was tested with several different configurations of DC Link capacitors. A special capacitor interface board was utilized to easily install and remove the capacitors. EMI measurements were taken across two ranges: (1) low frequency range (50 kHz - 200 kHz), and (2) high frequency range (150 kHz to 30 MHz).

A. EMI Isolation Bench

Fig. 6 shows the EMI test bench used in this research. A 600 V / 15 kW DC voltage source provides power to the device under test (DUT) via two CISPR 25 rated LISNs. The setup sits on top of a $4'$ x $8'$ copper ground plane. The DUT is a three phase inverter that is capable of swapping DC link capacitors in and out quickly. In total, six capacitors are connected in parallel to form the DC link. The flexibility of the test setup enables six new capacitors, six aged capacitors, or a combination of the two of them (i.e. intermediary classes) to be installed for the evaluation.

For each class of capacitors that was tested, the inverter operated under the same loading conditions; the parameters are given in Table II. Here, m_a is the modulation index, f_s is the switching frequency, and f_c is the fundamental frequency. Sine pulse width modulation (SPWM) was used to generate the AC output. It was fed into an R-L load. For all EMI data collected to train the SVM, the voltage across $R_{LISN,1}$ in Fig. 3 was measured using a spectrum analyzer.

TABLE II
Operating Parameters for the Experiment.

V_{DC}	I_{IN}	m_a	f_s (kHz)	f_c (Hz)	R_M (Ω)	L_M (μH)
540	7.1	.9	20	60	24	370

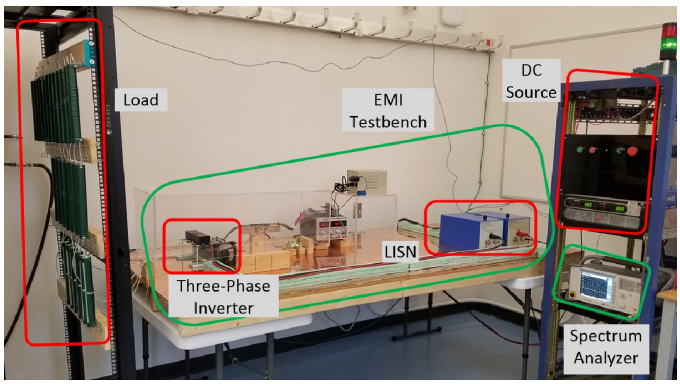

Fig. 6. EMI testbench used to collect experimental results.

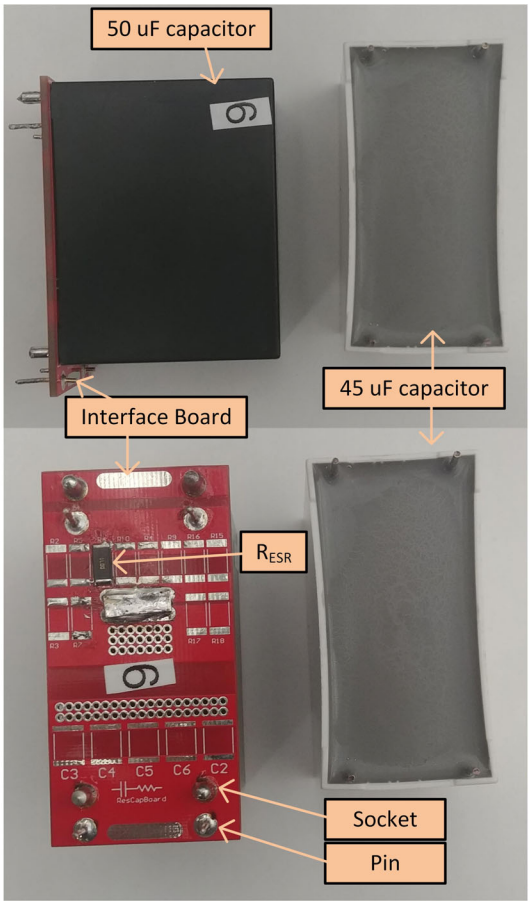

Fig. 7. Interface board used to emulate capacitor aging.

TABLE III
C_{DC} AND R_{ESR} FOR NEW AND AGED CAPACITOR CLASSES.

Class	new Capacitors	aged Capacitors
C_{DC}	50 μF	45 μF
R_{ESR}	7 $m\Omega$	24 $m\Omega$

TABLE IV
COMPOSITE DC LINK BUS FORMED FROM N_{Cnew} AND N_{Caged} CAPACITORS.

Class ID	N_{Cnew}	N_{Caged}
New	6	0
Partially aged	5	1
Half aged	3	3
Nearly aged	1	5
Aged	0	6

B. Capacitor Classes

Two distinct capacitor classes were used for this research. Both were created using commercial-off-the-shelf film capacitors. The new capacitors were implemented using 50 μF components (p/n: MKP1848C65090JY5 [19]), and the aged capacitors were created from 45 μF units (p/n: C4AEJBW5450A3MJ [20]). They are shown in Fig. 7. An interface board was created to enable the capacitors to be inserted and removed quickly. It also enables the R_{ESR} and capacitance to be increased. The interface board also enables fine adjustments, as well as substantial ones. The goal for future studies is to quantify the limitations of the EMI Diagnostic method versus slight variations in the DC Link's parameters.

The parameters of each capacitor class are shown in Table III. The values for this evaluation reflect those of a new capacitor bank and the same capacitor bank as it would appear after 3000 hours of operation. The analysis provided in [18] were used as a reference.

To train the SVM, a data set of either 25 or 49 EMI measurements were used to generate features. For the first capacitor class, the DC Link was created with six new capacitors. The second capacitor class was constructed using six of the aged capacitors in the DC Bus. Using only these samples, a single model was trained. Then new data was gathered and used to evaluate the accuracy of the SVM's ability to detect changes in the DC Link.

The evaluation data was collected differently than the data used to train the SVM. First, multiple measurements were made using the same setup consisting of a DC link using the first and second capacitor classes. In addition to this, samples were collected for capacitor banks containing a combination of capacitors from the new class and capacitors from the aged class. Table IV lists all combinations of capacitors used to test the model.

C. Data Acquisition

Two groups of tests were conducted. The first set focused on measurements around the resonant frequency of the DC link. An SVM model was created to analyze this data. The second set of measurements examined a range outside of the DC link resonant frequency.

For testing conducted in the 150 kHz - 30 MHz frequency range, 50 samples of EMI data were collected for the new capacitor class, the aged capacitor class, and each of the three intermediate classes. Four additional samples of the new capacitor class, and five additional samples of the aged capacitor class were collected on a different day, and under different conditions than the original data to test the robustness of the trained model.

For the 50 kHz - 200 kHz frequency range, 50 samples of EMI data were collected for the new capacitor class and the aged capacitor class. The model was trained using 25 of the samples from each class. The remaining 25 samples from each class were used to test the model. An additional 25 samples were collected from two intermediate classes. These results were also fed into the model and tested.

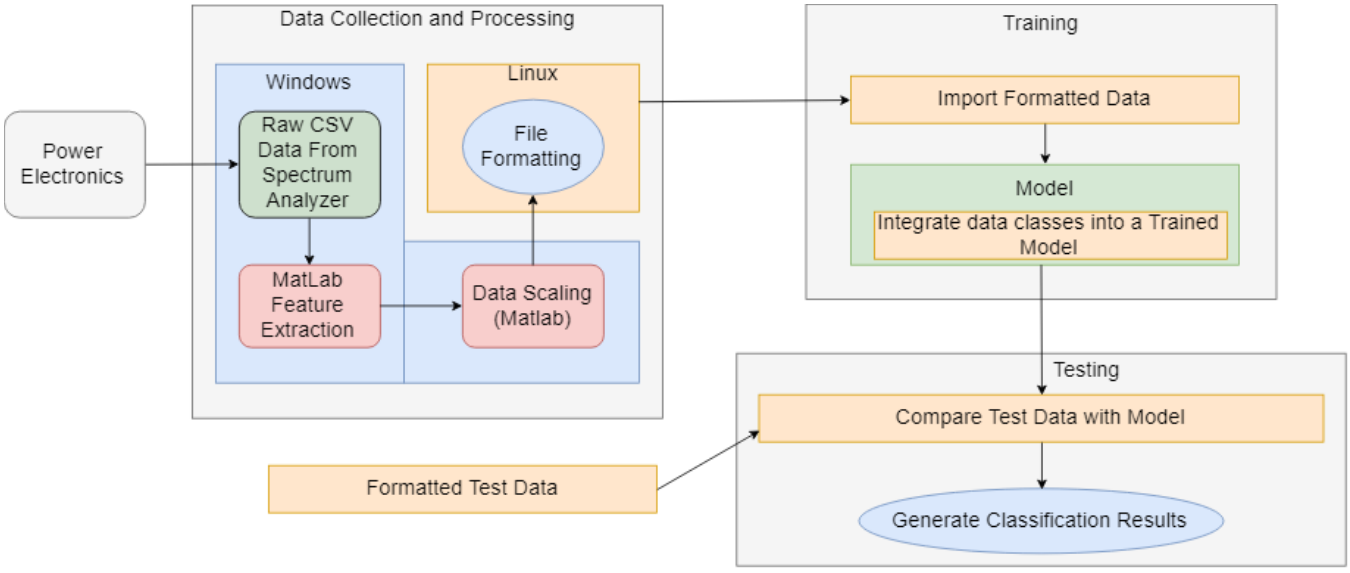

Fig. 8. Block Diagram used to describe data collection methods.

D. Feature Extraction

Fig. 8 shows the process used to extract features from the EMI data collected from a spectrum analyzer. Prior to extracting the features used by the SVM, all of the samples from a class were averaged together. Then, the difference of the two averages was computed. Fig. 9(a) shows the EMI spectrum of the new class and aged class in the 10 kHz to 200 kHz band, and Fig. 9(b) shows the differences between the two sets of measurements. (These images have been truncated and plotted on a linear x-scale to show the differences more clearly.) The features were extracted at the points where the difference between the two signals was the greatest. These features were selected because they represent the signal characteristics that can most accurately distinguish one class from the other. Fig. 9 highlights the features that were extracted by marking their frequencies with a black $+$ marker. The extracted features were then used as a data set describing each sample collected in the experiment and used to train a model. Once the model was trained, additional data sets were collected and classified using the model. The generated classification results determine the robustness of the model.

IV. Analysis

A. Common Mode and Differential Mode Results

Fig. 10 shows the common mode (CM) and differential mode (DM) EMI signals collected between 10 kHz to 200 kHz. One set of measurements was obtained using a DC link of only new capacitors and another was from a DC link with aged capacitors. It is clear that the CM EMI is similar for both capacitors classes above 100 kHz. This is to be expected as the DC link capacitor does not play a role in mitigating CM noise. The anomaly at 85 kHz still needs to be investigated.

The differences in the DM EMI measurements is more pronounced. With a high capacitance and lower R_{ESR}, the new capacitors do a better job of filtering the switching frequency harmonics. This difference is consistent with the theoretical analysis provided in Section II.

B. Model Verification and Cross Validation

The approach to train and test the SVM was different for the low frequency range (i.e. 10 kHz to 200 kHz) and the high frequency range (i.e. 150 kHz to 30 MHz). In the low frequency range, 50 samples were collected for each class. 25 of them were used to train the SVM. The other 25 of them were used to test the SVM.

For the high frequency range, a round-robin approach was implemented. The data collected for the model was verified by using a number samples within the model to train a sub model while using the remaining samples to test the sub model. For each sub model, 49 of the 50 samples from each class were used in training. The remaining sample from each class was then used to test the corresponding sub model. Every possible permutation of the data was used to sample a sub model containing 49 samples from each class, resulting in a total of 2500 trained sub models.

Table V shows an example of a hypothetical sub model containing a total of 100 samples from two classes. In Table V samples 1 and 53 are used to test the model, and the other 98 samples are used for training. A second example would be to use samples 1 and 54 for testing while the other 98 are used for training.

C. SVM Classification Results

For the 150 kHz - 30 MHz test, four trials of EMI data from the new capacitor class and five trials of EMI data from the aged capacitor class were used to test the models ability to classify strongly defined classes. The model was able to classify the nine trials with 77.8 % accuracy. The model incorrectly classified two of the new capacitor trials.

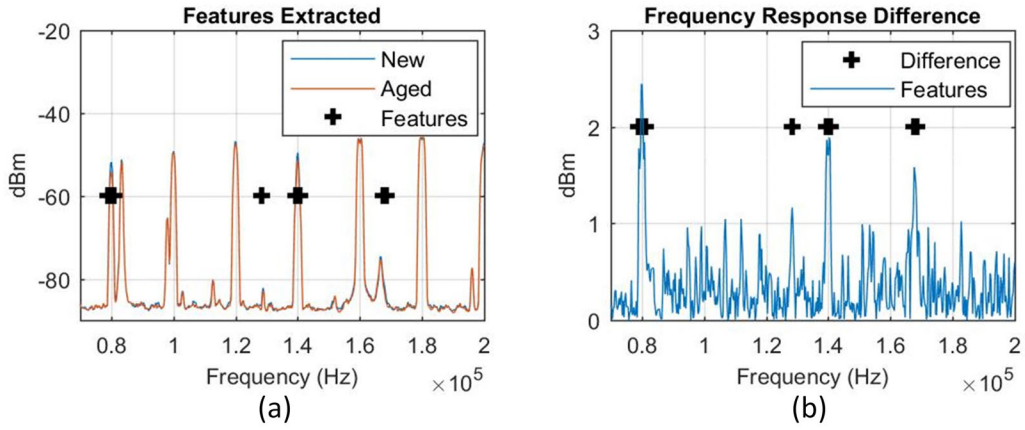

Fig. 9. EMI spectrum of the new and aged capacitor classes (a) and the features that were extracted from the point of greatest difference (b).

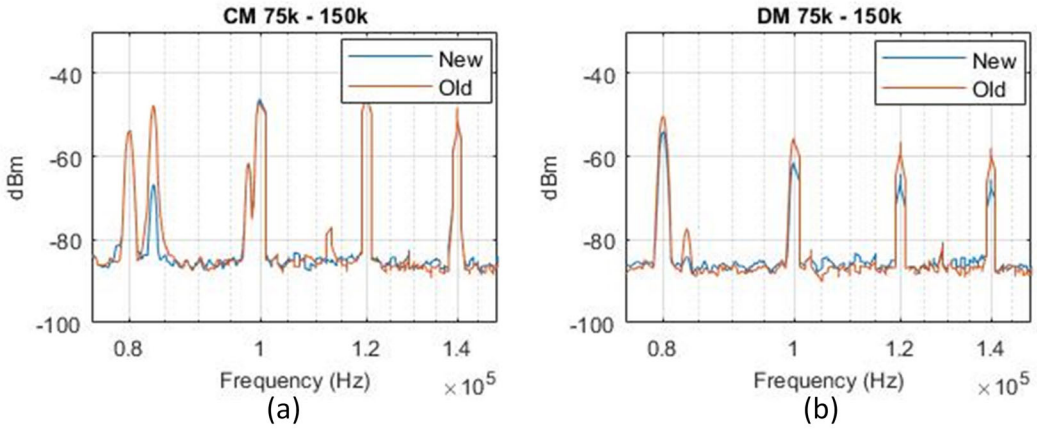

Fig. 10. EMI spectrum of the CM (a) and DM (b) EMI response in new and aged capacitor classes.

TABLE V
EXAMPLE OF A MODEL WHERE TRIALS 1 AND 53 ARE USED FOR TESTING.

Sample ID	Class ID	Model Relationship
1	New	Testing
2	New	Training
3	New	Training
...	...	...
51	Aged	Training
52	Aged	Training
53	Aged	Testing
...	...	...
100	Aged	Training

TABLE VI
RESULTS FOR INTERMEDIATE HEALTH CASES USING DATA FROM 150KHZ TO 30 MHZ

Class	Accuracy	Decision
Six New	50 %	New
Five New One Old	94 %	New
Three New Three Old	100 %	Aged
One New Five Old	100 %	Aged
Six Aged	100 %	Aged

The results of all testing in this frequency range for new, aged, and intermediate classes can be seen in Table VI.

For the 50 kHz - 200 kHz test, 25 trials of EMI data from the new capacitor class and 25 trials of data from the aged capacitor class were used to test the low frequency model. The model was able to classify the remaining 50 trials with 100 % accuracy. This suggests that the lower frequency data is able to more accurately describe the difference in EMI between each class. This observation reinforces the LCR data that was used to describe the difference in the capacitor impedance near the resonant frequency, and it suggests that these changes in the resonant frequency can be measured and classified using the EMI signals obtained from the DC side of a three phase inverter.

TABLE VII
RESULTS FOR INTERMEDIATE HEALTH CASES USING DATA FROM 50KHZ TO 200 KHZ.

Class	Accuracy	Decision
Six New	100 %	New
Five New One Old	100 %	Aged
Three New Three Old	100 %	Aged
Six Old	100 %	Aged

V. CONCLUSION

The following paper discusses using EMI as a diagnostic tool to determine the health of a DC link capacitor in a three phase inverter. It first explores how the C_{DC} and R_{ESR} change as a capacitor ages and how these changes impact the resonant frequency and impedance of the DC link capacitor. Then, it derives the transfer function for the DM noise in the circuit and uses it to demonstrate how variations in the DC link capacitance can be measured by LISNs. Lastly, it describes the experimental procedures that were followed and presents the results.

The findings suggest that EMI measurements can classify the health of the DC link capacitors in a three phase inverter. The results demonstrate that the SVM is able to accurately detect the capacitor changing by taking EMI measurements around the capacitor's resonant frequency. From the EMI spectrum, one can see that differences in the DM noise enable this method to work. Additionally, one can see that in the higher frequency band, it is more difficult to distinguish between the two classes of capacitors because the inductive reactance dominants. In future papers, the authors will quantify the limitations in the EMI diagnostics method and demonstrate using the high frequency range spectrum to identify other issues with components in a three phase inverter.

REFERENCES

[1] International Air Transport Association, Airline Maintenance Cost Executive Commentary. Montreal CA: Maintenance Cost Task Force, 2015

[2] U. PeriyarSelvam et al., Analysis on Costs for Aircraft Maintenance, Analysis on Costs for Aircraft Maintenance, vol. 3, no. 3, pp177-182, 2013.

[3] J. E. Timperley and J. M. Vallejo, "Condition Assessment of Electrical Apparatus With EMI Diagnostics," in IEEE Transactions on Industry Applications, vol. 53, no. 1, pp. 693-699, Jan.-Feb. 2017.

[4] R. T. Harrold, F. T. Emery, F. J. Murphy and S. A. Drinkut, "Radio Frequency Sensing of Incipient Arcing Faults within Large Turbine Generators," in IEEE Transactions on Power Apparatus and Systems, vol. PAS-98, no. 4, pp. 1167-1173, July 1979.

[5] F. T. Emery and R. T. Harrold, "On Line Incipient ARC Detection in Large Turbine Generator Stator Winding," in IEEE Transactions on Power Apparatus and Systems, vol. PAS-99, no. 6, pp. 2232-2240, Nov. 1980.

[6] M. Dlamini, P. S. Barendse and A. Khan, "Autonomous detection of interturn stator faults in induction motors," 2013 IEEE International Conference on Industrial Technology (ICIT), Cape Town, 2013, pp. 1700-1705.

[7] D. Casadei et al., "Detection of magnet demagnetization in five-phase surface-mounted permanent magnet generators," 2012 3rd IEEE International Symposium on Power Electronics for Distributed Generation Systems (PEDG), Aalborg, 2012, pp. 841-848.

[8] T. M. Wolbank, P. Nussbaumer, H. Chen and P. E. Macheiner, "Non-invasive detection of rotor cage faults in inverter fed induction machines at no load and low speed," 2009 IEEE International Symposium on Diagnostics for Electric Machines, Power Electronics and Drives, Cargese, 2009, pp. 1-7.

[9] X.-S. Pu, T. H. Nguyen, D.-C. Lee, K.-B. Lee, and J.-M. Kim, Fault diagnosis of DC-link capacitors in three-phase AC/DC PWM converters by online estimation of equivalent series resistance,IEEE Trans. Ind. Electron., vol. 60, no. 9, pp. 41184127, Sep. 2013.

[10] M. L. Gasperi, Life prediction modeling of bus capacitors in ac variable frequency drives, IEEE Trans. Ind. Appl., vol. 41, no. 6, pp. 14301435, Nov.-Dec. 2005.

[11] M. Markdessi, A. Sari, P. Venet, P. Bevilacqua and C. Joubert, Accelerated Aging of Metallized Film Capacitors Under High Ripple Currents Combined with a DC Voltage, IEEE Trans. Power Electron., vol. 30, no. 5, pp. 2435-2444, May 2015.

[12] J. Timperley and J. Vallejo, Condition Assessment of Electrical Apparatus With EMI Diagnostics, IEEE Trans. Ind. Appl., vol. 53, no. 1, pp.693-699, Mar. 2010.

[13] H. Wang and F. Blaabjerg, "Reliability of Capacitors for DC-Link Applications in Power Electronic ConvertersAn Overview," IEEE Trans. Ind. Appl., vol. 50, no. 5, pp. 3569-3578, Sept.-Oct. 2014.

[14] "Everything You Wanted To Know About Capacitors But Were Afraid To Ask", PSMA Capacitor Committee and IEEE PELS Capacitor Workshop, San Antonio, Texas, March 2018.

[15] C. Chen and X. Xu, "Modeling the conducted EMI emission of an electric vehicle (EV) traction drive," 1998 IEEE EMC Symposium. International Symposium on Electromagnetic Compatibility. Symposium Record (Cat. No.98CH36253), Denver, CO, 1998, pp. 796-801 vol.2.

[16] CISPR 25: Vehicles, Boats and Internal Combustion Engines-Radio Disturbance CharacteristicsLimits and Methods of Measurements for the Protection of On-board Receivers, IEC, third ed., 2008.

[17] A. Belousov, S. Verzakov, and J. von Frese, Applicational aspects of support vector machines, J. of Chemometrics, vol. 16, no. 8-10, pp. 482-489. Aug. 2002.

[18] C. Dublilier, L. Macomber, Apec 2011: Special Presentation 1.3.2 on Aluminum Electrolytic Capacitors. Applied Power and Energy Conversion Conf.. Mar. 2011, pp. 1-14.

[19] Vishay Roederstein, "Metallized Polypropylene Film Capacitors," Rep. no. MKP1848C65090JY5 Datasheet, Mar. 21, 2016.

[20] Kemet, "C4AE Series, Radial, 2 or 4 Leads, 450 - 1100 VDC, for DC Link," Rep. no. C4AEJBW5450A3MJ Datasheet, Mar. 3, 2017.